Available online at www.sciencedirect.com
SCIENCE DIRECT®
Advances in Space Research 37 (2006) 209–218
ADVANCES IN SPACE RESEARCH (a COSPAR publication)
www.elsevier.com/locate/asr

Observations of the solar soft X-ray irradiance by the student nitric oxide explorer

Scott M. Bailey [a,*], Thomas N. Woods [b], Francis G. Eparvier [b], Stanley C. Solomon [c]

[a] Geophysical Institute, Department of Physics, University of Alaska, 903 Koyukuk Dr., Fairbanks AK 99775, United States
[b] Laboratory for Atmospheric and Space Physics, University of Colorado, Boulder, CO 80303, United States
[c] High Altitude Observatory, National Center for Atmospheric Research, Boulder, CO 80307, United States

Received 25 March 2005; received in revised form 14 June 2005; accepted 18 July 2005

Abstract

The student nitric oxide explorer (SNOE) satellite made daily solar observations of the solar soft X-ray irradiance over most of the period from March 10, 1998 through March 16, 2002. Wavelengths below 30 nm, referred to as soft X-rays, were measured in broadband channels consisting of photodiodes with thin film filters deposited directly on the diode surfaces. SNOE had three such channels measuring in the bands 0.1–7, 6–19 , and 17–20 nm. The solar rotational (~27-day) variability in these bands is 44%, 28%, and 14%, respectively, and the solar cycle (11-year) variability is approximately factors of 11, 6 and 5, respectively. The SNOE observations are compared to more recent observations by the TIMED SEE instrument which uses the same technique at similar levels of solar activity and are found to be larger by a factor nearing two. The SNOE observations are shown however to be in excellent agreement with the EUVAC empirical model of solar irradiance.

Keywords: Solar irradiance; Soft X-ray; Solar variability

1. Introduction

The solar soft X-ray irradiance, here defined as 0.1–30 nm, is important in that it provides an energy source to the lower thermosphere and ionosphere for the production of photoelectrons which then produce E-region ionization, odd-nitrogen leading to the production of nitric oxide, and airglow emissions. Thus, the soft X-ray spectral region plays an important role in the ionospheric structure as well as in the energetic and chemical properties of the upper atmosphere. The solar soft X-ray irradiance is highly variable and is thus a significant driver of space weather. To understand the influence of the Sun on the atmosphere, it is vitally important to understand this region of the Sun's spectrum. The aeronomy community has been hindered in the past due to poor knowledge of this part of the sun's spectrum. Bailey et al. (2000, 2001) review the history of solar soft X-ray irradiance measurements as well as the use of those measurements in atmospheric models.

Observations by the student nitric oxide explorer (SNOE) brought about a significant improvement in our understanding of the solar soft X-ray irradiance. The Solar X-ray Photometer (SXP) on SNOE (Bailey et al., 2000, 2001) used new X-ray sensitive detectors (Bailey et al., 1999a) and precise calibrations with known synchrotron light sources at the National Institute of Standards and Technology (NIST) to measure the soft X-ray irradiance in three channels. Validation measurements were obtained with sounding rocket underflights of similar instrumentation being developed for the Solar EUV Experiment (SEE) on the Thermosphere Ionosphere Mesosphere Energetics and Dynamics

* Corresponding author. Tel.: +1 907 474 7741.
E-mail address: scott.bailey@gi.alaska.edu (S.M. Bailey).

0273-1177/$30
doi:10.1016/j.asr.2005.07.039

(TIMED) mission. TIMED was launched in December of 2001 and SEE has been observing the solar soft X-ray irradiance using the same technique as SNOE since that time (Woods et al., 2005).

Analysis of SNOE observations by Bailey et al. (1999b, 2000, 2001) confirmed earlier suggestions that the solar soft X-ray irradiance is larger than suggested by earlier measurements and empirical models (Hinteregger et al., 1981) by a factor of approximately four (and varying somewhat with solar activity). Solomon et al. (2001) used this scaling factor in an ionospheric model and showed that the SNOE solar soft X-ray observations allow for the first time agreement between observations and models of E-region electron densities and photoelectron fluxes. Barth and Bailey (2004) showed that the SNOE soft X-ray irradiances used in a photochemical model explain observed SNOE NO observations. Eastes et al. (2004) showed that the SNOE irradiances correlated well with thermospheric neutral densities obtained from satellite drag observations.

Lean et al. (2003) compared the newly developed NRLEUV physics based model of the solar irradiance and its variability to the two longest wavelength SNOE channels. They showed that the SNOE 17–20 nm irradiances were larger than the NRLEUV predictions by more than a factor of 2. Fox (2004) used a scaling factor to the Hinteregger et al. (1981) model similar to that used by Solomon et al. (2001) to compute electron and ion densities in the ionosphere of Mars. In comparing their results to observations, Fox concluded that the uniform scaling factor to Hinteregger irradiances below 20 nm was inappropriate and suggested that the scaling factors should be reduced at the longer wavelengths between 15 and 20 nm.

The present work extends on the earlier analysis of SNOE observations in three ways. The earlier works presented the first 1.5 years of data. In this paper, we present the full data set which spans most of four years. We will also make comparisons to the TIMED SEE observations. A third goal is to improve the interpretation of the SNOE broadband observations by using a new reference spectrum. This final goal directly addresses Fox's conclusions. Some preliminary comparisons of SNOE and SEE observations are discussed in Woods et al. (2004, 2005).

A detailed description of the SNOE measurement technique is provided in the following section. A key component of this analysis is that a reference spectrum must be used to interpret the broadband measurements. The broadband photodiodes produce currents which provide accurate descriptions of the energy impinging on their surfaces. To relate photodiode current to the solar spectrum requires assumptions about the wavelength of the impinging irradiance. If the assumed reference spectrum does not contain irradiance at short wavelengths, the inferred longer wavelength irradiances are increased to compensate for the missing irradiance. In the first analyses of SNOE and sounding rocket photodiode observations (Bailey et al., 1999a,b, 2000, 2001) the reference spectrum was taken from the model of Hinteregger et al. (1981). This empirical model has a short wavelength cutoff at 1.8 nm. It was therefore assumed that in non-flare conditions, there was negligible contribution from wavelengths shorter than 1.8 nm. Since these first analyses, new physics based modeling of the solar spectrum has been performed (Meier et al., 2002; Warren et al., 2001) and the results show significant irradiance below 1.8 nm. Neglecting irradiance at these wavelengths as done previously has the effect of artificially increasing the inferred irradiance at longer wavelengths. In the present analysis, we will incorporate the new reference spectrum in the SNOE analysis. The result of this analysis will be that the irradiances in the two long wavelength channels are reduced by approximately 50% from the results of Bailey et al. (2000, 2001). Minimal effect is seen on the shortest wavelength channel. This result is in qualitative agreement with Fox (2004).

2. Observations

SNOE was launched on February 27, 1998, into a 556 km near-circular Sun-synchronous orbit with an average local time of 10:30. It was a spinning satellite rotating at 5 rpm. Details of the mission, the scientific objectives, the spacecraft, its subsystems, and the instrumentation can be found in Bailey et al. (1996) and Solomon et al. (1996) (see also Barth and Bailey (2004)). SNOE made observations until November of 2003 and reentered the atmosphere on December 13 of that year. Because of the evolution of the SNOE orbit, solar observations were not possible after February 2002.

The SXP on the SNOE spacecraft performed photometric measurements of the solar soft X-ray irradiance in three selected wavelength channels. The channels consist of X-ray sensitive photodiodes with thin films deposited directly onto the active areas. Bailey et al. (2000, 2001) describe in detail the instrument, its operation, the data reduction algorithms, and the analysis of the first measurements.

An individual photometer bandpass is determined from thin-film filters deposited directly on a photodiode in the wafer form (Canfield et al., 1994; Bailey et al., 1999a,b). The particular material and thickness in conjunction with the uncoated photodiode response determine the wavelength region of sensitivity for each photometer. Each coating is designed to provide a narrow band of transmission when folded in with the bare photodiode sensitivity. In particular, the coatings must be thick enough to block any contribution from the much brighter long-wavelength spectrum of the Sun.

The use of three photometers with different filters yields the desired wavelength coverage. The combination of bare photodiode sensitivity, coating materials, and thicknesses of those materials determine the passband for each channel. The SNOE complement of photodiodes is listed in Table 1 along with the coating materials, their thicknesses, and wavelength range they were designed to measure. These ranges are determined by convolving the sensitivity of the coated diode with a solar reference spectrum as discussed in detail later.

Calibrations of the coated photodiodes were performed prior to launch using the Synchrotron Ultraviolet Radiation Facility (SURF II) at NIST at wavelengths longer than 5 nm (Canfield, 1987). In order to enhance the accuracy of the calibrations and extend the wavelength coverage below 5 nm the sensitivity is modeled based on the known sensitivity of a bare photodiode (Korde and Canfield, 1989; Canfield et al., 1994) and the calculated transmission of the thin-film filters. The NIST calibrations and the modeled sensitivity are shown in Fig. 1. The modeled sensitivity is used in the data processing. Bailey et al. (2000, 2001) discuss the calibration and the resulting uncertainties in greater detail. The measurements and the model predictions agree to within 5% at the primary wavelengths where the diodes are most sensitive. The NIST measurements have 1-σ relative uncertainties of 4–10%.

When observing the Sun at soft X-ray wavelengths with photodiodes, long wavelength (i.e., visible light) contributions to the measured signal must be accounted for. These contributions are present because the bare photodiodes are nearly as sensitive to visible light as they are to soft X-rays while the visible solar spectrum is many orders of magnitude brighter. The photodiode coatings are designed to be thick enough to block visible light; however, microscopic pinholes in the coatings pass enough visible light that they can produce a significant signal that must be subtracted from the data. This subtraction was made possible by the use of a fused silica window. A door mechanism on the SXP moved the fused silica window in front of the photometer channels. The fused silica passed UV and visible radiation but not soft X-ray or EUV. Therefore measurements made with the door closed give the magnitude of background signal that is due to long-wavelength radiation and any dark current. A correction must be made as the transmission of fused silica is slightly less than 100%. The transmissions of the filters are measured in the laboratory with a tungsten lamp and are typically ~94% at visible wavelengths. Degradation of the fused silica window in space was expected to be minimal; nonetheless, one uncoated SXP photodiode was used to measure the visible transmission of the window. Analysis of the degradation of the windows over the SNOE mission found that the window transmission degraded by about 10%. This has been accounted for in the processing.

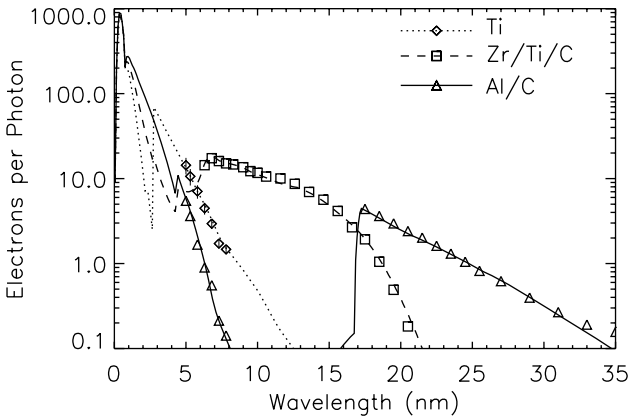

Fig. 1. Sensitivity of the coated SNOE photodiodes. Symbols are measurements made at the Synchrotron Ultraviolet Radiation Facility. Vertical lines over the symbols on the Ti values indicate 2-σ uncertainties for those measurements. The uncertainties for the other photodiodes are not shown because they are smaller than the sizes of the plotting symbols. The lines through the symbols are the modeled sensitivities based on the sensitivity of a bare photodiode and the transmissions of the thin film coatings.

The magnitude of the contribution of visible light to the observed signal is strongly dependent on incidence angle. This dependence occurs because the visible light signal is primarily due to pinholes in the coatings that are not spread uniformly across the active area. In fact, they tend to appear in the outer edges of the photodiode which only become illuminated at larger incidence angles. Thus large increases in the visible light signal are observed for angles of incidence approaching the edges of the $\pm 30°$ field of view. This variation in the visible light contamination with incidence angle is important since SNOE is a spinning satellite and solar observations

Table 1
SNOE channel information

	Channel 1	Channel 3	Channel 4
Coating	Ti/TiO	Zr/Ti/C	Al/C
Thicknesses (nm)	220/100	120/15/70	210/80
Signal below 10 nm (%)	98	50	35
Signal above 10 nm (%)	2	50	65
Available observations	3/11/1998 – 4/10/2001, 1/1/2002 – 3/17/2002	3/11/1998 – 9/12/1999, 11/25/1999 – 10/6/2000	3/11/1998 – 9/12/1999

are performed over a range of incidence angles. In this work observations within 15° of normal to the active area are considered. This feature of the instrument is accommodated in the data analysis by comparing only door open and door closed observations made at the same angles of incidence. See Bailey et al. (2000, 2001) for a full description of the instrument operation.

A component of the visible signal when the fused silica window is present in front of the photodiodes is due to reflections from the window itself. The fraction of visible light due to reflections was measured prior to flight as a function of incidence angle and is incorporated in the data reduction described next.

3. Data reduction to current units

The measurement samples are sorted according to the position of the Sun in the field of view. The visible light contributions to the measurements are subtracted, and the resulting current is then converted into solar irradiance units.

Removal of the visible light contribution to the measured current is accomplished by subtracting a door-closed (i.e., window in front of the photodiode) measurement from a door-open measurement in the following way:

$$C_{\mathrm{SXR}_i} = C_{\mathrm{open}_i} - \frac{C_{\mathrm{closed}_i}}{T_i}. \tag{1}$$

The subscript i denotes channel, C_{SXR} denotes counts per integration period which are due to solar soft X-rays, C_{open} denotes measured counts per integration period when the door was open, and C_{closed} denotes measured counts per integration period when the door was closed. These observations are made at identical incidence angles so that the variation of the visible light background with incidence angle is implicitly accounted for. The transmission T_i of the window is determined for each observation from the ratio of door-closed and door-open measurements taken from the uncoated photodiode (again at identical incidence angles) denoted with a subscript u

$$T_i = \frac{C_{\mathrm{closed}_u}}{C_{\mathrm{open}_u}} f_i. \tag{2}$$

The factor f_i is the preflight-measured factor that accounts for light that reflected off the photodiode and then reflected from the window back onto the diode surface.

The remaining signal after subtracting the visible light signal is then converted to current units, nanoamperes per m^2, using the conversion factor measured prior to launch and the known active area of the photodiode. The resulting currents are due only to solar soft X-ray irradiance.

4. Interpreting the measured currents to determine the solar irradiance

The measurements are now converted into irradiance units. In order to perform this conversion a solar reference spectrum and the sensitivity of the photodiode are convolved and integrated to produce a reference current. The ratio of the measured current to the reference current is defined as the scaling factor for the reference spectrum over the bandpass of the photodiode. The scaling factor is calculated according to:

$$\mathrm{SF}_i = \frac{I_{\mathrm{SXR}_i}}{I_{\mathrm{ref}_i}} = \frac{I_{\mathrm{SXR}_i}}{\sum_j S_i(\lambda_j) F(\lambda_j)}, \tag{3}$$

where SF_i is the scale factor for channel i, I_{SXR_i} is the soft X-ray current measured by channel i, I_{ref_i} is the soft X-ray current predicted by the reference spectrum, $S_i(\lambda_j)$ is the sensitivity of channel i at wavelength j, and $F(\lambda_j)$ is the model irradiance at wavelength j. Note that the full reference spectrum is used in calculating the reference current. In order to calculate irradiance, the scaling factor is applied to the reference spectrum and the scaled spectrum is integrated over the photodiode's bandpass. The photodiode bandpasses are described below. This process is done for each photodiode individually. The results are reported in energy units ($\mathrm{mW\ m^{-2}}$). Energy units are optimal for the SXP results because a silicon photodiode current is proportional to the impinging energy flux (1 e^- hole pair per 3.63 eV energy).

5. Reference spectrum

The reference spectrum used in previous analyses of the SNOE data was produced by the empirical model of Hinteregger et al. (1981) which is based on the SC#21REFW solar minimum reference spectrum. The Hinteregger model covered the range 1.8–102.7 nm and takes the daily F10.7 and the 81-day average of the daily F10.7 values as input parameters. The model was run each day for the conditions appropriate to that day. A limitation of this reference model is the lack of any information below 1.8 nm. It was previously assumed that irradiance below 1.8 nm produced a negligible current in the SXP channels. Recent physics based modeling of solar irradiance by Warren et al. (2001) have produced a new reference spectrum. This spectrum extends below 2 nm and has been used in interpreting observations by TIMED SEE (Woods et al., 2005). Note that this spectrum was first used by Meier et al. (2002) in order to study the effects on the Earth's atmosphere of the enhancement of the solar soft X-ray irradiance during the flare of April 21, 2002. The spectrum we use here is the pre-flare quiet time spectrum used in that study.

The SNOE channel sensitivities have been convolved with this new spectrum. These convolutions are shown

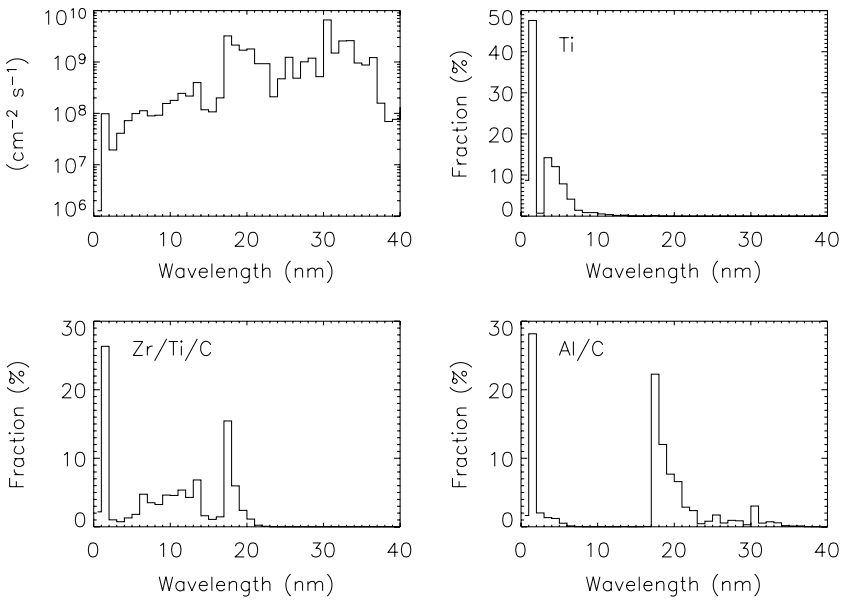

Fig. 2. Convolutions of the photodiode sensitivities with the reference solar spectrum. The convolutions are shown in 1-nm bins. For each bin the fraction of the total signal produced from that wavelength bin in percent is plotted. The upper left panel shows the reference spectrum. The upper right panel is for the Ti coated photodiode. The lower panes are for the Zr/Ti/C and Al/C coated photodiodes, respectively.

in Fig. 2. The photodiode sensitivities convolved with the reference spectrum illustrate which wavelengths generate the bulk of the soft X-ray current generated by each photodiode when viewing the Sun. It is these convolutions that are used to determine the bandpass of each photometer channel. The convolutions are shown in units of percent of total current in 1-nm intervals. As an example of how to interpret the figure, for the Ti-coated photodiode, Channel 1, 48% of the total signal comes from solar irradiance in the 1–2 nm interval, while 90% of the signal from the 0–7 nm interval. Note that while a very small amount of the current is produced at wavelengths longer than 7 nm, we declare the photodiode bandpass as 0.1–7 nm. This is because for longer wavelengths, significant changes in the solar spectrum produce negligible changes in the total measured current, and therefore the measured current may not be indicative of the brightness of the Sun at those wavelengths. Contributions outside the declared bandpass are still considered.

In Channel 3, the Zr/Ti/C coated photodiode, the primary bandpass is 6–19 nm. In the Al/C coated photodiode, the primary bandpass is 17–20 nm. Both of these have significant components of their signals from wavelengths below 7 nm (see Table 1). These contributions were ignored in previous analyses of SNOE observations. In order to compensate for this signal in these two channels, Eq. (3) above is modified. The results of using Eq. (3) for Channel 1 are used to calculate the current at wavelengths shorter than the primary bandpass in Channels 3 and 4. This signal can then be subtracted off before the scaling factor of the reference spectrum at the longer wavelength bandpass is calculated. Thus, for Channels 3 and 4, Eq. (3) is modified to

$$\mathrm{SF}_i = \frac{I_{\mathrm{SXR}_i} - I_S}{I_{\mathrm{ref}_i}} = \frac{I_{\mathrm{SXR}_i} - I_S}{\sum_j S_i(\lambda_j) F(\lambda_j)}, \tag{4}$$

where I_S is the current produced by wavelengths shorter than the primary bandpass. This current is calculated from the results of analysis of Channel 1 from

$$I_{S_i} = \sum_j \mathrm{SF}_1(\lambda_j) S_j F(\lambda_j) S_i, \tag{5}$$

where SF_1 is the scaling factor determined from Channel 1 and S_i is the sensitivity of Channel i. The sum in Eq. (5) is taken over the shortest wavelengths outside the primary bandpass of the channel. The sum in Eq. (4) is taken over all longer wavelengths.

Uncertainties in the derived irradiances from the above procedures are due to uncertainties in the calibrations, errors of line ratios in the assumed solar spectrum, and random errors in the measurements. The random errors play a role four times as the soft X-ray current is the result of a difference measurement (Eq. (1)) and a ratio (Eq. (2)). The relative uncertainties in the calibrations including measurements and the application of the modeled sensitivity are ~10% (Bailey et al., 2000, 2001). Errors in the line ratios of the assumed reference solar spectrum are not easily quantified but are assumed to be no larger than 15%. The largest source of error is the component introduced in subtracting the visible light background. The resulting uncertainty from this source is quantified by examining the standard deviation about

the mean current measurement from each observing period. The standard deviation in the Ti-coated photodiode data (0.1–7 nm) is typically ~20% and for the Zr/Ti/C and Al/C photodiode data (6–19 and 17–20 nm) ~ 10% (Bailey et al., 2000, 2001). All of the above uncertainties are 1-σ values. The total root-mean-square uncertainty is on average 27% for the Ti measurements and 21% for the Zr/Ti/C and Al/C photodiodes.

6. Results

The dates of observations for each channel are listed in Table 1. Between September and November of 1999, the gain in the electronics of Channels 3 and 4 began to drift. Changes in gain can be quantified by comparing visible light measurements (door closed) made at identical viewing angles. By 25 November 1999, Channel 3 settled into a stable gain and functioned fully until October of 2000. The gain in Channel 4 continued to drift.

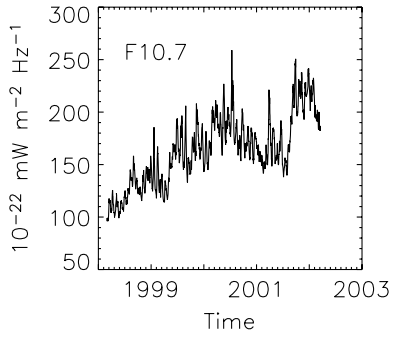

Fig. 3. Solar activity index for the time period of the SNOE observations. The values shown are an equally weighted average of the daily and the 81-day mean of the 10.7 cm solar irradiances.

The time dependent gain in this channel is likely recoverable through a careful comparison of daily visible light measurements made before and after the gain began to change. That analysis has not been completed at this time. Channel 1 never suffered any changes in gain as determined by analyzing visible light measurements throughout the mission. After April 10 of 2001, the SNOE orbit had deteriorated in such a way that it was not always possible to make both solar and Earth observations. Channel 1 observations were made between January 1 and March 16 of 2002 and then solar observations were not made again. These gain changes are thought to be caused by energetic particles damaging the detector electronics.

In order to put the SNOE observations in perspective, the solar F10.7 index for the time period of SNOE observations is shown in Fig. 3. The F10.7 index is known to correlate well with the solar soft X-ray irradiance (Bailey et al., 2000 and references therein). For such comparisons we use the average of the daily F10.7 and the 81-day average of the F10.7 index. It is this value that is plotted in Fig. 3. This index has shown the best correlations with the SNOE observations and is used in the remainder of this paper. Fig. 3 shows that the solar cycle had an early peak in 2000 and a second larger peak at the end of 2001 and beginning of 2002.

Fig. 4 shows the SNOE irradiance results derived from the observations described above and interpreted using the procedure outlined earlier. The irradiances are appropriate to the energy ranges listed in Table 1 and in the figure. As in Fig. 3, the general features of the rise to solar maximum and the 27 day solar rotation variability are seen in the data. The SNOE Channel 1 observations show the early peak very well and capture the end and decline of the later peak. A statistical estimate of the 27-day variability is obtained by taking

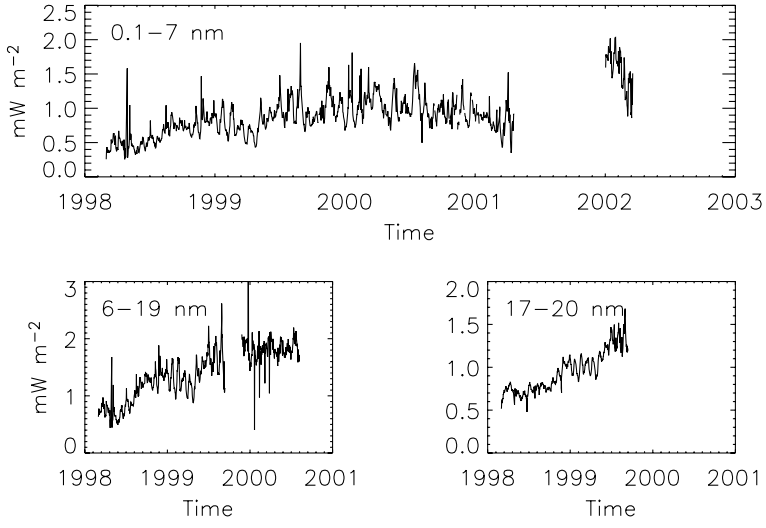

Fig. 4. Daily soft X-ray irradiance measurements for the full SNOE mission.

twice the standard deviation of the ratio of the daily irradiance to the 81 day average of the irradiance. The determined 27-day variability of the 0.1–7 nm irradiance is then approximately 44%. For the 6–19 nm irradiance, the 27-day variability is 28%, and by 17–20 nm the 27-day variability is reduced to approximately 14%.

Fig. 5 shows the SNOE irradiances as a function of F10.7. SNOE made observations in the range of F10.7 levels about 95–230. In the case of the 17–20 nm channel, the highest values of F10.7 are about 200. SNOE observed the 0.1–7 nm irradiance vary between 0.3 to values as high as 2.0 mW m^{-2}. The present results agree to within 10% of the results presented by Bailey et al. (2000, 2001) over the period of overlap. The new reference spectrum adjusts how the irradiance is distributed within the 0.1–7 nm bandpass, but cannot affect the total energy contained within it. The new results for the 6–19 nm irradiance show it to vary from about 0.5 to 2.2 mW m^{-2} and the 17–20 nm irradiance from about 0.5 to 1.5 mW m^{-2}. These results are both about 50% lower than the results presented by Bailey et al. (2000, 2001) in the time period of overlap. This change is due to the realization from the new reference spectrum described earlier that a significant amount of the observed photodiode current is produced by short wavelength irradiance outside the primary bandpass.

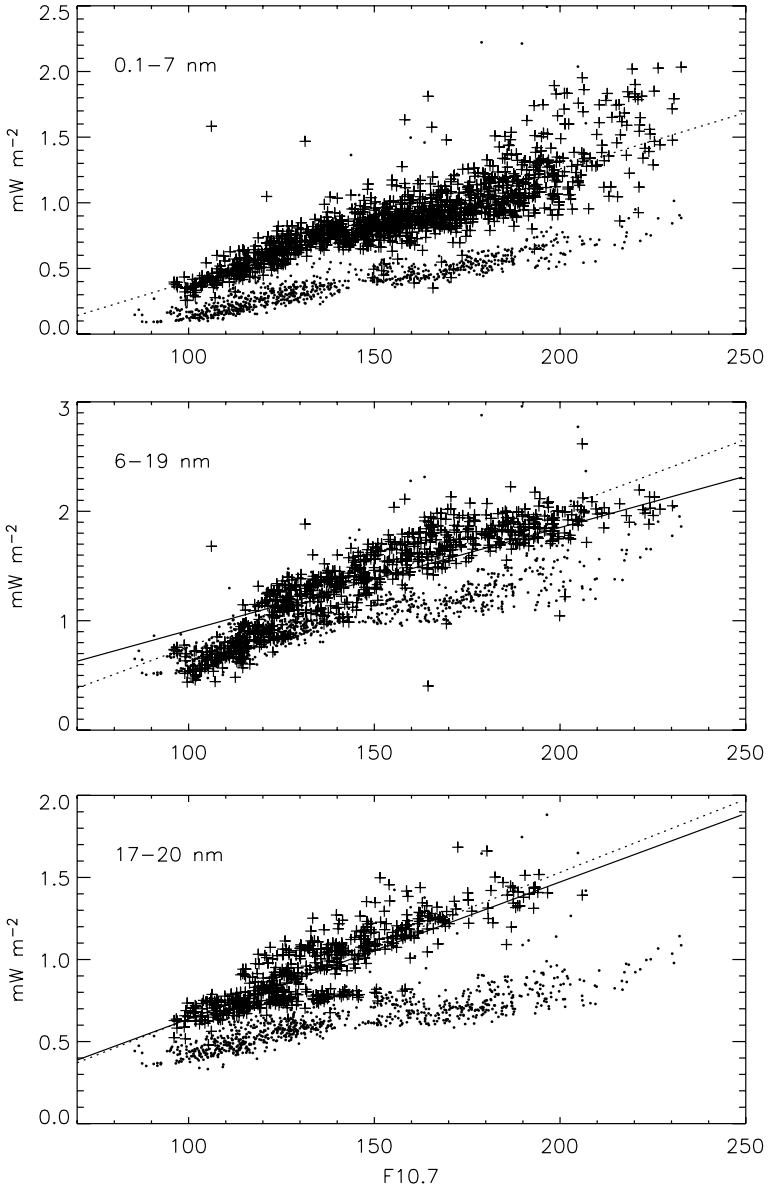

Fig. 5. Observed irradiances as a function of F10.7 in each of the three SNOE bands. Plus symbols are the SNOE observations. Small dots are SEE observations. The dashed line is the result of a linear fit of SNOE observations to F10.7 index. The solid line is the EUVAC prediction of the solar irradiance in the same wavelength intervals. In both the figures and the fits, the F10.7 index used is the average of the daily and 81-day running mean values.

Table 2
Linear fit parameters to SNOE irradiances

Wavelength (nm)	Intercept	Slope	Value at F10.7 = 70	Value at F10.7 = 230	Ratio	27-day Var. (%)
0.1–7	−0.46	0.0086	0.14	1.52	10.9	44
6–19	−0.50	0.0126	0.38	2.40	6.2	28
17–20	−0.25	0.0089	0.37	1.80	4.9	14

In Fig. 5, linear fits are drawn through the SNOE data. The observations are well represented by linear fits with correlation coefficients on the order of 0.8 in all three bands. The scatter is larger at the larger solar activities and there is a hint of curvature at the low levels of solar activity. The fit parameters are listed in Table 2. These fits can be used to estimate the solar minimum and solar maximum values of the soft X-ray irradiance in the three bands. These are also listed in Table 2. Approximating solar minimum by F10.7 = 70 and solar maximum by F10.7 = 230, we see that the 0.1–7 nm irradiance ranges from 0.14 to 1.52 mW m^{-2} for a solar cycle variability of a factor of 10.9. The 6–19 nm irradiance ranges from 0.38 to 2.40 mW m^{-2} for a variation of a factor of 6.2, and the 17–20 nm irradiance ranges from 0.37 to 1.8 mW m^{-2} for a variation of a factor of 4.9.

7. Comparison to observations by SEE and the EUVAC empirical model

As mentioned earlier, the SNOE observations are made with a technique identical to that employed by the SEE instrument on the TIMED spacecraft. SEE began observing in January 2002 and observations continue to the present. SEE has made measurements at similar levels of solar activity as SNOE. The V7 SEE data are plotted with the SNOE data as a function of F10.7 in Fig. 5. While the variability appears to be similar, the magnitudes are clearly different. The SEE data are lower than the SNOE data by approximately a factor of two.

To quantify the differences between SNOE and SEE, we examine the mean values from each instrument as a function of solar activity. These are obtained by taking all points in a range of F10.7 at a specified value plus and minus 10. These mean values are listed in Table 3. In the 0.1–7 nm range, SNOE is larger than SEE by a factor of 2.0 ± 0.3. There is no clear trend in the ratios and this is true for each of the bands. In the 6–19 nm range, SNOE is larger than SEE by a factor of 1.3 ± 0.2, and in the 17–20 nm range, SNOE is larger than SEE by a factor of 1.6 ± 0.2.

Bailey et al. (2000, 2001) concluded that the SNOE observations were in approximate agreement with sounding rocket underflights of the SEE prototype instrument. By inference then it would be reasonable to conclude that SNOE should be in agreement with SEE observations. Since the work of Bailey et al. (2000, 2001), lab testing of the spare photodiodes from the SEE program have been recalibrated at the SURF III facility at NIST. Unlike the SNOE calibrations, these new calibrations were performed with a different beamline and viewed the synchrotron directly as opposed to through a monochrometer and compared to a reference detector. Woods et al. (2005) describe these calibrations and the technique used to determine the photometer responsitivity between 1 and 40 nm, being at shorter wavelengths than the SNOE SURF II calibrations down to 5 nm. These new SEE calibrations resulted in changes in the photodiode sensitivities at short wavelengths on the order of a factor of 2 and are included in the SEE observations presented here. Although the uncertainties from both experiments are on the order of 20–30%, which can nearly explain the difference, we conclude that it is the changes in the SEE calibration that are the primary driver of the differences described above. Both programs use the same reference spectrum for

Table 3
Comparison of SNOE and SEE irradiances

F10.7	0.1–7 nm			6–19 nm			17–20 nm		
	SNOE	SEE	Ratio	SNOE	SEE	Ratio	SNOE	SEE	Ratio
100	0.42	0.16	2.60	0.65	0.66	0.98	0.67	0.45	1.50
120	0.59	0.27	2.17	0.99	0.86	1.16	0.82	0.55	1.48
140	0.79	0.40	1.97	1.33	1.04	1.28	1.00	0.65	1.54
160	0.89	0.50	1.77	1.62	1.17	1.38	1.18	0.71	1.66
180	1.04	0.57	1.81	1.83	1.28	1.44	1.36	0.75	1.81
200	1.24	0.70	1.77	1.88	1.44	1.31	1.42	0.84	1.70
220	1.52	0.67	2.28	2.01	1.42	1.42			
Mean			2.0			1.3			1.6
Std. dev.			0.3			0.2			0.2

interpreting the data and so it is not possible that the reference spectrum leads to the discrepancies. Spare photodiodes from the SNOE program exist and may be recalibrated at SURF III in the future. Until that happens, the discrepancies between SNOE and SEE will remain.

An alternative method of comparing SNOE and SEE observations is to compare their differing predictions in separate studies on the effects of the solar irradiance on the atmosphere. Example possibilities include the modeling of photoelectron fluxes escaping from the atmosphere as described by Woods et al. (2003), other ionospheric parameters as described by Solomon et al. (2001), or even planetary ionospheres as described by Fox (2004).

It is also useful to compare the two datasets to existing empirical models of the solar soft X-ray irradiance. The EUVAC empirical model (Richards et al., 1994) is such a model and has been used in several aeronomical studies. The EUVAC model predicts irradiance as a function of F10.7 in the wavelength range 5–102 nm. Thus comparisons are not possible in the 0.1–7 nm band. In this comparison, a new version of the model (Richards, 2005, private communication) which predicts irradiance in selectable wavelength bins (0.1 nm in this case) is used. Other than the binning format there are no significant changes to the model.

In the two longer wavelength bands, Bailey et al. (2000, 2001) found reasonable agreement with EUVAC. In the present analysis assuming the NRLEUV spectrum and the improved short wavelength sensitivity, the agreement has improved. As shown in Fig. 5, the EUVAC prediction overlaps the SNOE observations. The slope is slightly different in the 6–19 nm channel, but the agreement is excellent in the 17–20 nm band. In contrast the results from SEE observations, Mars ionosphere analysis (Fox, 2004), and NRLEUV model predictions (Lean et al., 2003) suggest lower irradiance values.

Further effort in understanding the difference between SNOE and SEE is required. The calibrations of the two sets of photodiodes should be compared and if possible, the spare photodiodes should undergo identical calibrations. Further modeling studies as mentioned above should also take place. Spectral measurements of the solar soft X-ray irradiance may help understand the discrepancies in the broadband measurements and would greatly improve our interpretation of those observations.

8. Conclusions

We have provided a time series of solar soft X-ray irradiance measurements in the 0.1–7, 6–19 , and 17–20 nm bands. The observations are made using an instrument consisting of a set of photodiodes with thin film filters deposited directly on their surfaces. Analysis of these bands shows 27-day rotation variability ranging from 44% at the shortest wavelengths to 14% at the longest wavelengths. The observed solar cycle variability ranges from factors of 11 at the short wavelengths to 5 at the longest wavelengths. The irradiances are seen to vary nearly linearly with F10.7 as an indicator of solar activity. Observations were made over the range of F10.7 of 95–230. The SNOE observations show similar variability to similar observations by TIMED SEE, but with a magnitude a factor of 1.3–2 larger. This discrepancy is attributed to revisions in the SEE calibrations using spare photodiodes calibrated at the new SURF III facility after the launch of SEE and transferred to the SEE flight photometers using the solar observations from an underflight rocket experiment. Similar calibrations with spare SNOE photodiodes may be possible. The SNOE data are shown to be in excellent agreement with the EUVAC empirical model of solar irradiance.

References

Bailey, S.M., Barth, C.A., Erickson, M.J., Kohnert, R.A., Merkel, A.W., Rodgers, E.M., Solomon, S.C., Straight, S.D., Vian, J.E., Woods, T.N. Science instrumentation for the student nitric oxide explorer. Proc. SPIE Int. Soc. Opt. Eng. 2830, 264, 1996.

Bailey, S.M., Woods, T.N., Canfield, L.R., Korde, R., Barth, C.A., Solomon, S.C., Rottman, G.J. Sounding rocket measurements of the solar soft X-ray irradiance. Sol. Phys. 186, 243, 1999a.

Bailey, S.M., Woods, T.N., Barth, C.A., Solomon, S.C. Measurements of the solar soft X-ray irradiance from the student nitric oxide explorer. Geophys. Res. Lett 26, 1255, 1999b.

Bailey, S.M., Woods, T.N., Barth, C.A., Solomon, S.C., Korde, R., Canfield, L.R. Measurements of the solar soft X-ray irradiance by the student nitric oxide explorer: first analysis and underflight calibrations. J. Geophys. Res. A 105 (12), 27179, 2000.

Bailey, S.M., Woods, T.N., Barth, C.A., Solomon, S.C., Korde, R., Canfield, L.R. Correction to Measurements of the solar soft X-ray irradiance by the student nitric oxide explorer: first analysis and underflight calibrations. J. Geophys. Res. A 106 (8), 15791, 2001.

Barth, C.A., Bailey, S.M. Comparison of a thermospheric photochemical model with SNOE observations of nitric oxide. J. Geophys. Res., doi:10.1029/2003JA010227, 2004.

Canfield, L.R. New far UV detector calibration facility at the National Bureau of Standards. Appl. Opt. 26, 3831, 1987.

Canfield, L.R., Vest, R., Woods, T.N., Korde, R. Proc. SPIE Int. Soc. Opt. Eng. 2282, 31, 1994.

Eastes, R., Bailey, S.M., Bowman, B., Marcos, F., Wise, J., Woods, T.N. The correspondence between thermospheric neutral densities and broadband measurements of the total solar soft X-ray flux. Geophys. Res. Lett., doi:10.1029/2004GLO20801, 2004.

Fox, J.L. Response of the Martian thermosphere/ionosphere to enhanced fluxes of solar soft X-rays. J. Geophys. Res. A 109 (11310), doi:10.1029/2004JA010380, 2004.

Hinteregger, H.E., Fukui, K., Gilson, G.R. Observational, reference and model data on solar EUV from measurements on AE-E. Geophys. Res. Lett. 8, 1147, 1981.

Korde, R., Canfield, L.R. Silicon photodiodes with stable near theoretical quantum efficiency in the soft X-ray region. Proc. SPIE Int. Soc. Opt. Eng. 1140, 126, 1989.

Lean, J.L., Warren, H.P., Mariska, J.T., Bishop, J. A new model of solar EUV irradiance variability. 2., Comparisons with empirical models and observations, and implications for space weather. J. Geophys. Res. 108 (A2), 1059, 2003.

Meier, R.R., Warren, H.P., Nicholas, A.C., Bishop, J., Huba, J.D., Drob, D.P., Lean, J.L., Picone, J.M., Mariska, J.T., Joyce, G., Judge, D.L., Thonnard, S.E., Dymond, K.F., Budzein, S.A. Ionospheric and dayglow responses to the radiative phase of the Bastille Day flare. Geophys. Res. Lett., 29, doi:10.1029/2001GLO13956, 2002.

Richards, P.G., Fennelly, J.A., Torr, D.G. EUVAC: A solar EUV flux model for aeronomic calculations. J. Geophys. Res., 99, 1994.

Solomon, S.C., Barth, C.A., Axelrad, P.A., Bailey, S.M., Brown, R., Davis, R.L., Holden, T.E., Kohnert, R.A., Lacy, F.W., McGrath, M.T., O'Conner, D.C., Perich, J.P., Reed, H.L., Salada, M.A., Simpson, J., Srinivasan, J.M., Stafford, G.A., Steg, S.R., Tate, G.A., Westfall, J.C., White, N.R., Withnell, P.R., Woods, T.N. The Student Nitric Oxide Explorer. Proc. SPIE Int. Soc. Opt. Eng 2810, 121, 1996.

Solomon, S.C., Bailey, S.M., Woods, T.N. Effect of solar soft X-rays in the lower ionosphere. Geophys. Res. Lett. 28, 2149, 2001.

Warren, H.P., Mariska, J.T., Lean, J. A new model of solar EUV irradiance variability. 1. Model formulation. J. Geophys. Res. 106, 15745, 2001.

Woods, T.N., Bailey, S.M., Peterson, W.K., Warren, H.P., Solomon, S.C., Eparvier, F.G., Garcia, H., Carlson, C.W., McFadden, J.P. Solar extreme ultraviolet variability of the X-class flare on April 21, 2002 and the terrestrial photoelectron response. Space Weather 1, 1001, doi:10.1029/2003SW000010, 2003.

Woods, T.N., Acton, L.W., Bailey, S.M., Eparvier, F.G., Garcia, H., Judge, D., Lean, J., McMullin, D., Schmidtke, G., Solomon, S.C., Tobiska, W.K., Warren, H.P. Solar extreme ultraviolet and X-ray irradiance variations. in: Pap, J., Frshlich, C., Hudson, H., Kuhn, J., McCormack, J., North, G., Sprig, W., Wu, S.T. (Eds.), Solar Variability and Its Effect on Earth's Atmospheric and Climate System, Geophys. Monograph, vol. 141. American Geophysical Union, doi:10.1029/141GM11, 2004.

Woods, T.N., Bailey, S.M., Woodraska, D., Eparvier, F.G., Lean, J., Chamberlin, P., Rottman, G.T., Solomon, S.C., Tobiska, W.K. The solar EUV experiment (SEE): mission overview and first results. J. Geophys. Res. 110 (A01312), doi:10.1029/2004JA010765, 2005.